JVST A
Journal of Vacuum Science & Technology A

Operating modes and target erosion in high power impulse magnetron sputtering

Cite as: J. Vac. Sci. Technol. A **40**, 043005 (2022); https://doi.org/10.1116/6.0001919
Submitted: 15 April 2022 • Accepted: 25 May 2022 • Published Online: 21 June 2022

M. Rudolph, N. Brenning, H. Hajihoseini, et al.

COLLECTIONS

EP This paper was selected as an Editor's Pick

View Online

Export Citation

CrossMark

ARTICLES YOU MAY BE INTERESTED IN

On the population density of the argon excited levels in a high power impulse magnetron sputtering discharge
Physics of Plasmas **29**, 023506 (2022); https://doi.org/10.1063/5.0071887

High power impulse magnetron sputtering discharge
Journal of Vacuum Science & Technology A **30**, 030801 (2012); https://doi.org/10.1116/1.3691832

Review Article: Stress in thin films and coatings: Current status, challenges, and prospects
Journal of Vacuum Science & Technology A **36**, 020801 (2018); https://doi.org/10.1116/1.5011790

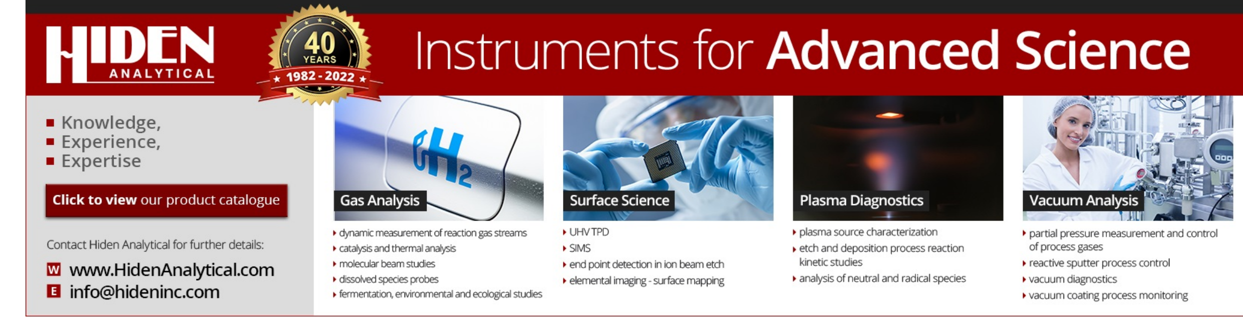

© 2022 Author(s).

Operating modes and target erosion in high power impulse magnetron sputtering

Cite as: J. Vac. Sci. Technol. A **40**, 043005 (2022); doi: 10.1116/6.0001919
Submitted: 15 April 2022 · Accepted: 25 May 2022 ·
Published Online: 21 June 2022

View Online Export Citation CrossMark

M. Rudolph,[1] N. Brenning,[2,3] H. Hajihoseini,[4] M. A. Raadu,[2] J. Fischer,[3] J. T. Gudmundsson,[2,5] and D. Lundin[3]

AFFILIATIONS

[1]Leibniz Institute of Surface Engineering (IOM), Permoserstraße 15, 04318 Leipzig, Germany
[2]Space and Plasma Physics, School of Electrical Engineering and Computer Science, KTH Royal Institute of Technology, SE-10044 Stockholm, Sweden
[3]Plasma and Coatings Physics Division, IFM-Materials Physics, Linköping University, SE-581 83 Linköping, Sweden
[4]Industrial Focus Group XUV Optics, MESA+ Institute for Nanotechnology, University of Twente, Drienerlolaan 5, 7522 NB Enschede, The Netherlands
[5]Science Institute, University of Iceland, Dunhaga 3, IS-107 Reykjavik, Iceland

ABSTRACT

Magnetron sputtering combines a glow discharge with sputtering from a target that simultaneously serves as a cathode for the discharge. The electrons of the discharge are confined between overarching magnetic field lines and the negatively biased cathode. As the target erodes during the sputter process, the magnetic field strengthens in the cathode vicinity, which can influence discharge parameters with the risk of impairing reproducibility of the deposition process over time. This is of particular concern for high-power impulse magnetron sputtering (HiPIMS) as the discharge current and voltage waveforms vary strongly with the magnetic field strength. We here discuss ways to limit the detrimental effect of target erosion on the film deposition process by choosing an appropriate mode of operation for the discharge. The goal is to limit variations of two principal flux parameters, the deposition rate and the ionized flux fraction. As an outcome of the discussion, we recommend operating HiPIMS discharges by maintaining the peak discharge current constant.

© 2022 Author(s). All article content, except where otherwise noted, is licensed under a Creative Commons Attribution (CC BY) license (http://creativecommons.org/licenses/by/4.0/). https://doi.org/10.1116/6.0001919

I. INTRODUCTION

Magnetron sputtering is a physical vapor deposition technique[1] that combines a glow discharge with sputtering a target which simultaneously serves as a cathode. When operating such a discharge in pulsed mode, high peak discharge currents can be achieved, while keeping the average power to the target below the maximum thermal load of the cathode target, a process referred to as high-power impulse magnetron sputtering (HiPIMS).[2] The high discharge currents increase the electron density during the pulse by two to three orders of magnitude compared to direct current magnetron sputtering (dcMS),[2] which leads to significant ionization of the film-forming species.[2–4]

The ions of the sputtered material contribute to the growth process by supplying additional energy to the surface, producing well-adhering and dense coatings.[5–7] The ionized flux fraction describes the fraction of ions in the flux of film-forming species toward the substrate. In HiPIMS, it is typically found to be in the range of 10–60%, and increases with increased discharge current density,[8–10] but also higher ionized flux fractions of up to 70% have been reported.[11]

The ions are produced in the so-called ionization region, which is the brightly glowing torus in the vicinity of the cathode target, in which electrons are trapped by the static magnetic field of the magnetron assembly. Some of the cathode potential falls over this region, forming an electric field directed toward the cathode. As a consequence, a fraction of ions produced in this region are back-attracted toward the cathode target, rather than contributing to the deposition rate. The probability of target ion back-attraction during the pulse-on time $\beta_{t,pulse}$ is rather high and usually lies between 50% and close to 100% and appears to depend on the target material,[12] along with operating parameters such as working gas pressure, discharge current, pulse length, etc.[10] This high probability that a target ion produced in the ionization region is

© Author(s) 2022

back-attracted onto the target is the dominant effect behind the frequently observed loss in deposition rate when comparing a HiPIMS discharge with a dcMS discharge at equal average power.[6] The low deposition rate is a commonly known drawback for HiPIMS processes.[13]

Optimization of HiPIMS discharges taking into account the two flux parameters, deposition rate and ionized flux fraction, is, therefore, recommended. Brenning *et al.* propose an optimization scheme for HiPIMS discharges.[10] It is based on the observation that the deposition rate and the ionized flux fraction cannot be maximized independently of each other but are rather strongly coupled and is referred to as the "HiPIMS compromise." They reveal that the target ion escape probability $(1-\beta_t)$ is a suitable figure of merit for HiPIMS discharges, in such a way, that a maximized $(1-\beta_t)$ allows the best possible combination of deposition rate and ionized flux fraction. In a first step, therefore, externally adjustable process parameters, such as the magnetic field strength in the ionization region, the working gas pressure, and the pulse length, need to be adjusted in order to maximize $(1-\beta_t)$. The recommendation is to use the weakest magnetic field strength[9] and the lowest working gas pressure[8,14] under the condition that a discharge can still be ignited. In addition, they recommend using a short pulse length.[15,16] In a second step, the ionized flux fraction is tuned by adjusting the peak discharge current density (see, e.g., Fig. 1 in Brenning *et al.*[10]). As the deposition rate scales inversely with the ionized flux fraction, given a constant ion escape probability $(1-\beta_t)$, the goal in this step is to keep the ionized flux fraction to the minimum value required to obtain the desired material properties.

The procedure above helps finding the "sweet spot" in which to operate a HiPIMS discharge. We note, however, that to keep the discharge in the defined process window by maintaining a constant ionized flux fraction and deposition rate is not trivial. This is due to the magnetic field that is strongly varying in the ionization region. The magnetic field is typically generated by two permanent magnet packs that are located behind the cathode target. One is located in the center and the other at the outer edge of the cathode, in such a way that the magnetic field lines form arcs above the cathode. The primary purpose of this magnetic field topology is to trap electrons, thereby increasing their residence time close to the target, which ultimately enables the sustainment of the discharge at a lower working gas pressure and lower discharge voltage compared to diode sputtering.[17] The magnetic field enables Ohmic heating of the electrons outside the cathode sheath and thereby enables a lower discharge voltage compared to diode sputtering.[18–20] The specific arrangement of the magnets in a magnetron assembly results in an increasing magnetic field strength when approaching the target surface. As the target erodes, the discharge moves into regions of stronger magnetic field, which can influence discharge parameters and impair the reproducibility of a deposition process over time.[21]

Here, we discuss changes in two flux parameters relevant for thin film deposition, the ionized flux fraction and deposition rate, as a function of the magnetic field strength to investigate the effect of an eroding target. The objective is to recommend a mode of operation for HiPIMS discharges that limits the variation of these two flux parameters. The three modes of operation studied here are the fixed pulse power mode, the fixed voltage mode, and the fixed peak current mode, which are defined in Sec. II. Measurements of the ionized flux fraction and deposition rate at six different positions above the cathode target surface are described in Sec. III and the implications of the results are discussed in Sec. IV. We conclude Sec. IV with a recommendation for the preferred mode of operating a HiPIMS discharge, before we summarize the main findings of the study in Sec. V.

II. OPERATING MODES IN HiPIMS

Operating a magnetron sputtering discharge, in particular, a HiPIMS discharge, involves controlling many discharge parameters, most of which are not independent from each other. For example, for a given working gas pressure and pulse length, the peak discharge current, the discharge voltage, and the magnetic field strength cannot be chosen independently from each other. When the discharge voltage is kept constant, the peak discharge current increases with a stronger magnetic field. Similarly, when the peak discharge current is kept constant, the discharge voltage decreases with a stronger magnetic field.[9] A mode of operation of a HiPIMS discharge is here defined by a discharge parameter that is maintained constant over time. For the modes studied here, electrical parameters are chosen because these can easily be measured and adjusted. Furthermore, we use electrical discharge parameters that define the properties of individual pulses: the discharge current $I_D(t)$, the discharge voltage $V_D(t)$, and two combinations of these parameters based on their time-integrated products. The first combination is the time-averaged discharge power,

$$\langle P_{av}\rangle = \frac{1}{T}\int_T I_D(t)V_D(t)\mathrm{d}t, \tag{1}$$

where T is the pulse period. The second combination is the pulse-averaged power, also termed the pulse power,[20,22]

$$\langle P_{pulse}\rangle = \frac{1}{t_{pulse}}\int_{t_{pulse}} I_D(t)V_D(t)\mathrm{d}t, \tag{2}$$

where t_{pulse} is the pulse length.

Three different ways of controlling the input power to the discharge follow from this discussion. The experimenter can set the power supply either to, first, maintain a constant pulse power over time, a mode that we here abbreviate by "fixed pulse power." This is the only mode available in pulsing units from the beginning of the HiPIMS development. These pulsers are based on thyristors and contain small capacitors, which are charged with a certain energy, and completely discharge during one pulse, releasing that energy.[23] The repetition frequency of these pulsing units is often fixed at 10 or 50 Hz.[11,24] The usually small capacitors in these power supplies result in large variations in the discharge current and voltage waveforms during the pulse (see, e.g., the waveforms reported in earlier studies[11,23,25]). A second mode, here abbreviated by "fixed voltage," regulates the power supply to maintain a constant discharge voltage. This mode is possible with modern power supplies containing sufficiently large capacitors to maintain the discharge voltage during the pulse at a close-to-constant value.[12,23] A third mode uses the

© Author(s) 2022

discharge current to regulate the power supply. As the discharge current is a strongly varying parameter during the pulse, one usually measures its peak value during the pulse and sets the power supply to maintain that value constant over time. The mode is here abbreviated by the term "fixed peak current."

The time-averaged discharge power is somewhat special, in a way that it can be adjusted largely independent from the other three regulating parameters. By adjusting the repetition period, the time-averaged discharge power can be varied without affecting the parameters peak discharge current, discharge voltage, and pulse power. The possibility to independently adjust the time-averaged discharge power and one of the other three parameters applies as long as the off-time between pulses is sufficiently long to avoid the interaction of two sequential pulses[15] (see, e.g., also the discussion on interacting pulses in chopped HiPIMS by Barker *et al.*[26,27] and Antonin *et al.*[28]). If independency applies, we suggest to always adjust the repetition frequency in order for the average power to equal the maximum allowable thermal load on the cathode target, as this increases the process throughput.

III. EXPERIMENTS

The goal of the experiments is to obtain variations in the ionized flux fraction and deposition rate as a function of the magnetic field strength in order to investigate the effect of an eroding target. Ideally, this would be done for the three modes of operation identified in Sec. II. However, we note that from these modes of operation, the fixed voltage mode and the fixed peak current mode are the two extreme cases. In the fixed pulse power mode, both the discharge voltage and current are adjusted simultaneously and, therefore, do not reach the extreme values obtained in fixed voltage and fixed peak current mode. The deposition rate and ionized flux fraction in the fixed pulse power mode can, therefore, be expected to lie in between the fixed voltage and the fixed peak current mode. For this reason, we experimentally study only the two extreme cases. From these measurements, the ionized flux fraction and deposition rate with strengthening of the magnetic field in the fixed pulse power mode can be estimated, provided the control algorithm of the power supply is known.

A. Experimental description

Here, we extend a study reported by Hajihoseini *et al.*[9] In this work, the authors studied HiPIMS discharges with a 4 in. titanium target, 6 mm in thickness, with argon as the working gas at 1 Pa, for a range of magnetic field configurations. They measured the deposition rate using a quartz crystal microbalance (QCM) and the ionized flux fraction using an ion meter, which is a charge-selective QCM (Refs. 8, 30). The measurements were done using the two modes of operation mentioned above, fixed voltage and fixed peak current. More details on the experimental setup are given elsewhere (Refs. 9, 29).

For the discussion here, we use a partially different set of measurements from the same experimental campaign. The deposition rate and ionized flux fraction were both measured using an ion meter to ensure consistency between the two parameters. In addition, the flux parameters were measured at three radial positions, above the center of the target ($r = 0$ cm), above the racetrack of the target ($r = 3$ cm), and above the edge of the target ($r = 5$ cm), and at two different heights above the target, at $z = 3$ cm and $z = 7$ cm. In all cases, the ion meter was facing the cathode target, thus measuring the axial flux of film-forming species leaving the ionization region. From the measurements, we derived the deposition rate of neutral film-forming species R_{tn} separately from the deposition rate of the ionic film-forming species R_{ti}.

The ionized flux fraction was then calculated by[4,14]

$$F_{\mathrm{flux}} = \frac{R_{\mathrm{ti}}}{R_{\mathrm{tn}} + R_{\mathrm{ti}}}. \tag{3}$$

The second parameter of interest was the deposition rate calculated by summing the individual deposition rates of target ions R_{ti} and neutrals R_{tn}, respectively,

$$R_{\mathrm{dep}} = R_{\mathrm{tn}} + R_{\mathrm{ti}}. \tag{4}$$

The magnetic field topology was changed by varying the distance between the center and edge magnet packs from the rear of the target surface. For all magnetic field configurations, the magnetic field strength was measured above the racetrack at 11 mm from the target surface. As the height of the ionization region was estimated to be around 2 cm, the measurement of the magnetic field strength was approximately in the center of the ionization region. When the two magnet packs were positioned closest to the rear of the target (termed C0E0 by Hajihoseini *et al.*[9]), the magnetic field strength was $B_{\mathrm{rt}} = 23.8$ mT. With both magnet packs at a distance of 10 mm from the rear of the target (termed C10E10), the magnetic field strength was $B_{\mathrm{rt}} = 11.1$ mT.

Target erosion leads to an increase in the local magnetic field strength at the target surface. In our experimental data, moving both magnet packs toward the rear of the target by 10 mm corresponds to an increase from the weakest to the strongest magnetic field, i.e., from 11.1 to 23.8 mT. We here assume that moving the magnets toward the target by a certain distance corresponds to eroding the target to the same depth Δz_{rt}. Note that there are typically two parameters that define a magnetic field of a magnetron assembly, the magnetic field strength and the position of the magnetic null point z_{null}, where the latter characterizes the degree of magnetic unbalance for type II magnetron assemblies.[31,32] Here, we base our analysis on the field strength only.

B. Experimental results

Table I summarizes the obtained discharge voltages V_{D} in the fixed peak current mode and the peak discharge currents $I_{\mathrm{D,peak}}$ in the fixed voltage mode as a function of the magnetic field strength B_{rt} in the ionization region. It is obvious that the relative changes in the peak discharge current, when operating the discharge in the fixed voltage mode, are much stronger compared to the changes in the discharge voltage, when operating the discharge in the fixed peak current mode. Increasing the magnetic field strength from 11.1 to 23.8 mT increases the peak discharge current from 12 to 80 A in the fixed voltage mode, i.e., by almost 570%. In the fixed peak current mode, the discharge voltage decreases only by 20%, when excluding the data point at the lowest magnetic field strength

© Author(s) 2022

TABLE I. Variations of V_D in the fixed peak discharge current ($I_{D,peak}$ = 40 A) mode and of $I_{D,peak}$ in the fixed voltage V_D = 625 V) mode. Please note that the relative variations are much larger in the bottom line (changes in $I_{D,peak}$ in fixed voltage mode) than in the middle line (changes in V_D in the fixed peak current mode). Data reproduced from Hajihoseini *et al.* [9]

B_{rt} (mT)	11.1	13.7	16.1	18.1	21.3	21.7	23.8
Fixed peak current mode							
V_D (V) ($I_{D,peak}$ = 40 A)	—	660	655	557	650	565	510
f (Hz)	—	99	97	129	111	123	143
Fixed voltage mode							
$I_{D,peak}$ (A) (V_D = 625 V)	12	31	36	53	35	54	80
f (Hz)	450	134	97	80	115	76	54

(11.1 mT), where the discharge did not reach the desired peak discharge current of 40 A.

The increasing magnetic field strength also influences the ionized flux fraction F_{flux}. Figure 1 shows the variation of F_{flux} in both fixed peak current and fixed voltage mode at three different locations within the discharge (above the center, above the racetrack, and above the edge of the target) and at two different heights ($z = 7$ and 3 cm above the cathode target surface). An additional axis in panel (a) indicates the equivalent change of erosion depth Δz_{rt}. Straight line fits show the trends of F_{flux} with an increasing magnetic field strength corresponding to a certain target erosion depth.

For the fixed voltage discharges, a significant increase in F_{flux} with increased magnetic field strength can be observed. This increase lies between 170% and 400% for all six measurement positions (Fig. 2), where the percentage change is measured on the linear fits from Fig. 1 to eliminate effects of data scattering.

On the other hand, the fixed peak current discharges show a decrease in F_{flux} with increased magnetic field strength. Note that in order to keep the change in F_{flux} comparable to the fixed voltage cases, we have extrapolated the data to a magnetic field strength of 11.1 mT. The extrapolation is indicated by the dotted line in Fig. 1. The relative changes in F_{flux} measured from that fit between the weakest ($B_{rt} = 11.1$ mT) and the strongest ($B_{rt} = 23.8$ mT) magnetic field values are $\Delta F_{flux} = -41\%$ and -45% for the measurements made above the center and the edge of the cathode target at a height of $z = 7$ cm, respectively. The relative change is only $\Delta F_{flux} = -3\%$ for the measurement done at $z = 3$ cm above the racetrack. These values for ΔF_{flux} are considerably smaller compared to the change in the ionized flux fraction ΔF_{flux} from target erosion when operating the discharge in the fixed voltage mode. We, therefore, conclude that the fixed peak current mode appears to be a better mode of operating a HiPIMS discharge compared to the fixed voltage mode in terms of maintaining F_{flux} constant under the influence of a strengthening magnetic field from target erosion.

The second parameter of interest is the deposition rate. Figure 3 shows the variation in the deposition rate as a function of the magnetic field strength. At all positions measured, we observe a considerable drop in the deposition rate with increasing target erosion for the fixed voltage cases. Contrary, for the fixed peak current cases, a slight increase in the deposition rate is observed for a strengthening magnetic field with target erosion. These changes are summarized in Fig. 4.

Note that Hajihoseini *et al.*[9] observed a decrease in the deposition rate for stronger magnetic fields, when operating the discharge in the fixed peak current mode. We attribute this discrepancy to the different measurement devices used. They measured their deposition rates using a quartz crystal microbalance, while we report here measurements using an ion meter, which has a reduced acceptance cone due to the specific setup of the magnetic shielding (see, e.g., Fig. 1 in Kubart *et al.*[30]). In addition, the measurements reported by Hajihoseini *et al.*[9] were made at a peak discharge current of $I_{D,peak} = 80$ A, while the measurements reported here were made at 40 A. On the other hand, comparing the deposition rates from discharges run in the fixed voltage mode (both done at $V_D = -625$ V), the results reported here match quite well with those reported earlier by Hajihoseini *et al.*[9] While they report a decrease in the deposition rate by 53% measured at a distance of $z = 7$ cm above the center of the racetrack, we observe a decrease of 43% (Fig. 4).

From the measurements reported in this work, we conclude that the deposition rate changes with a strengthening of the magnetic field from target erosion. The trend and magnitude depend on the mode of operation of the HiPIMS discharge. While for the fixed voltage discharges, a decrease in $\Delta R_{dep} \approx -40$ % to -50 % is observed, the fixed peak current discharges only show a slight increase of roughly 10% (Fig. 4). These results suggest the peak discharge current mode to be superior compared to the fixed voltage mode in terms of keeping the deposition rate constant with a changing magnetic field strength from target erosion.

IV. DISCUSSION

To understand the changes in the ionized flux fraction F_{flux} under two different modes of operation, we note that F_{flux} can be written analytically as[4]

$$F_{flux} = \left(1 + \frac{\xi_{tn}}{\xi_{ti}} \frac{1 - \alpha_t}{\alpha_t(1 - \beta_t)}\right)^{-1}. \tag{5}$$

It, thus, depends on three parameters from the material pathways model.[33,34] The first two are internal discharge parameters of the ionization region, the probability of target atom ionization,

$$\alpha_t = 1 - \frac{\int_T \Gamma_{tn}^{DR} dt}{\int_T \Gamma_{sput} dt}, \tag{6}$$

and the probability of target ion back-attraction,

$$\beta_t = 1 - \frac{\int_T \Gamma_{ti}^{DR} dt}{\int_T \Gamma_{sput} dt - \int_T \Gamma_{tn}^{DR} dt}, \tag{7}$$

where Γ_{tn}^{DR} and Γ_{ti}^{DR} are the fluxes [in (s^{-1})] of neutrals and ions out of the ionization region toward the diffusion region (i.e., not to the target), respectively, Γ_{sput} is the sputtered flux (in [s^{-1}]) from the target into the ionization region, and the integrals are over one pulse repetition period T.[4]

The third parameter concerns the flux of species from the ionization region to the substrate and is described by the ratio of

© Author(s) 2022

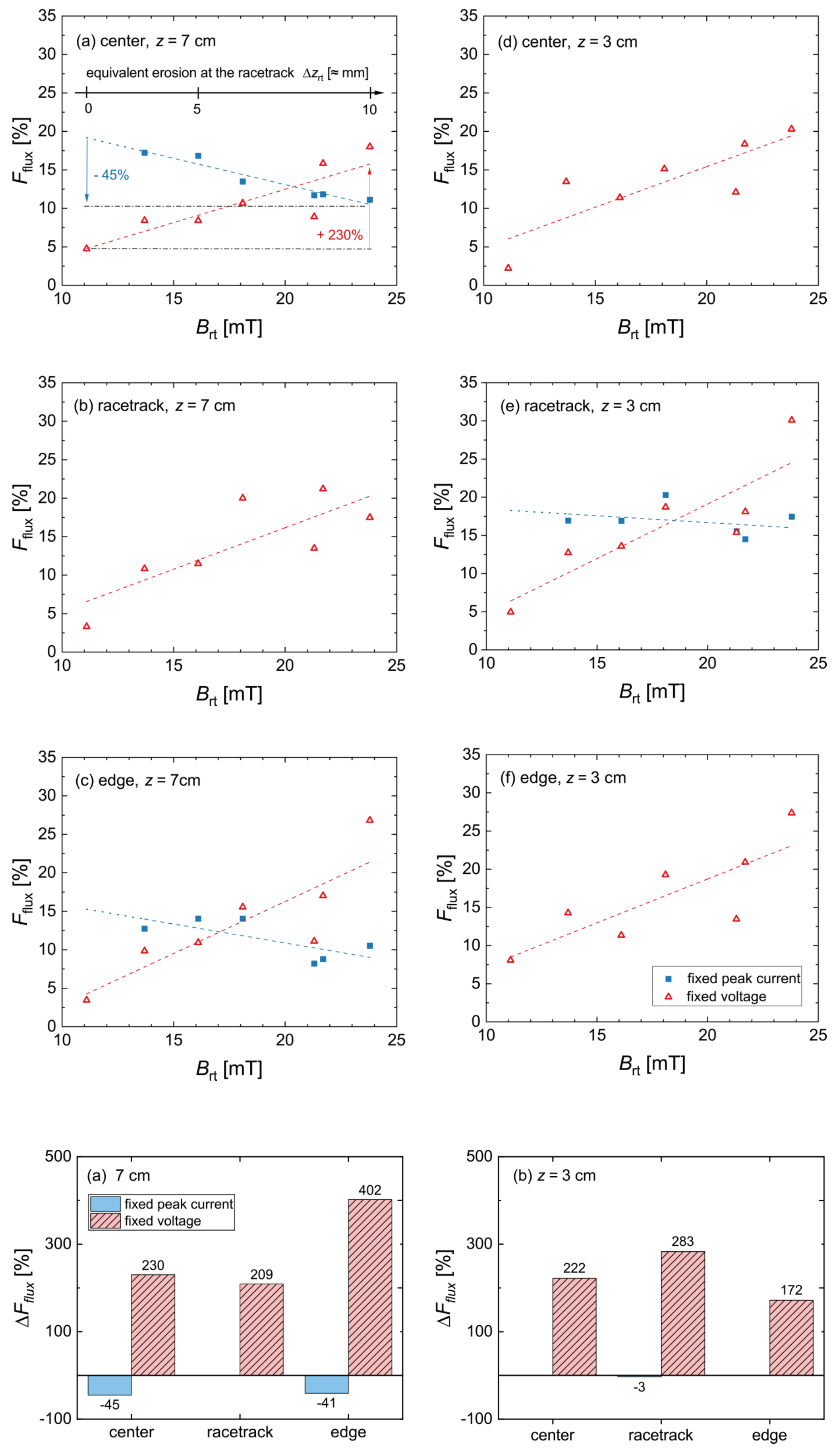

FIG. 1. Ionized flux fraction F_{flux} measured at a height of $z = 7$ cm (left column) above the (a) center, (b) racetrack, and (c) edge of the cathode target and at a height of $z = 3$ cm (right column) above the (d) center, (e) racetrack, and (f) edge of the cathode as a function of magnetic field strength B_{rt} measured at the racetrack position 11 mm above the cathode target surface.

FIG. 2. Effect of target erosion on F_{flux}. The plot shows the variation ΔF_{flux} for the fixed peak current and fixed voltage mode operated discharges measured at a height of (a) $z = 7$ cm and (b) $z = 3$ cm above the target surface. The change is measured from the fits in Fig. 1 between the weakest magnetic field configuration with $B_{rt} = 11.1$ mT (corresponding to an uneroded target) and the strongest magnetic field configuration with $B_{rt} = 23.8$ mT (corresponding to an erosion depth of $\Delta z_{rt} = 10$ mm).

© Author(s) 2022

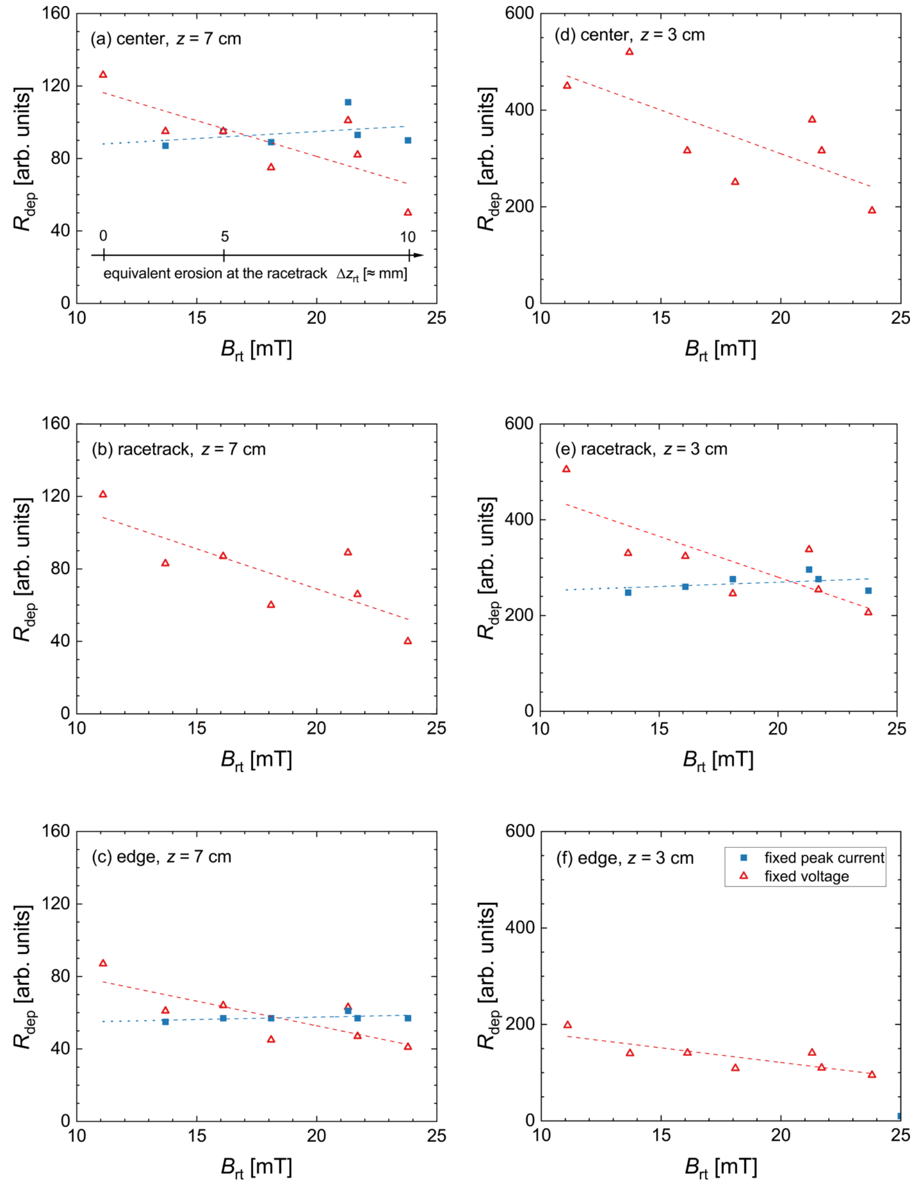

FIG. 3. Deposition rate R_{dep} measured at a height of $z = 7$ cm (left column) above the (a) center, (b) racetrack, and (c) edge of the cathode target and at a height of $z = 3$ cm (right column) above the (d) center, (e) racetrack, and (f) edge of the cathode target as a function of magnetic field strength B_{rt} measured at the racetrack position 11 mm above the cathode target surface.

transport parameters ξ_{tn}/ξ_{ti}.[14,33,34] The transport parameters ξ_{tn} and ξ_{ti} are the fractions of the target neutrals and target ions that leave the ionization region toward the diffusion region and deposit onto the substrate:[4] $\xi_{tn} = \int_T \Gamma_{tn}^{sub} dt / \int_T \Gamma_{tn}^{DR} dt$ and $\xi_{ti} = \int_T \Gamma_{ti}^{sub} dt / \int_T \Gamma_{ti}^{DR} dt$. Note that both ξ_{tn} and ξ_{ti} are functions of the substrate position, its size, and its orientation.[4]

Changes in the ionized flux fraction ΔF_{flux} can, thus, be traced back to changes in the two internal discharge parameters α_t and β_t and the ratio of the transport parameters ξ_{tn}/ξ_{ti}. We start discussing the F_{flux} values for the discharges in the fixed voltage mode, for which we observe an increasing value of F_{flux} with the stronger magnetic field. The key to understand this trend is that the discharges in the fixed voltage mode show an increasing peak discharge current for stronger magnetic fields (Table I). It is known that the electron density scales with the discharge current due to the necessity to match the discharge current with the ion current at the target.[20] As the sputtered atoms pass through this electron cloud in the ionization region on their way to the diffusion region, the probability of target atom ionization α_t grows. For the discharges studied here, α_t is known from an earlier study in which we used the Ionization Region Model (IRM), a global plasma-chemistry model, to extract internal discharge parameters for these particular discharges.[4] For example, $\alpha_t = 0.45$ for the discharge with the weakest magnetic field configuration ($I_{D,peak} = 12$ A), while $\alpha_t = 0.84$ for the discharge with the strongest magnetic field configuration

© Author(s) 2022

($I_{D,peak} = 80$ A). Figure 5 is replotted from Rudolph *et al.*[20] and shows the increase in α_t with increasing $I_{D,peak}$.

Equation (5) can be used to evaluate the significance of an increasing α_t on F_{flux}. Values for β_t and ξ_{tn}/ξ_{ti} can be taken from the modeling study mentioned above.[4] Here, we are interested only in a rough estimate, therefore, we use an average value for β_t of 0.85 and $\xi_{tn}/\xi_{ti} = 2$. Inserting the values $\alpha_t = 0.45$, $\beta_t = 0.85$, and $\xi_{tn}/\xi_{ti} = 2$ into Eq. (5), we obtain a value for $F_{flux} = 6\%$ for the discharge with the weakest magnetic field configuration. Using $\alpha_t = 0.84$ yields $F_{flux} = 28\%$ for the discharge with the strongest magnetic field configuration. These need to be compared with the values in Fig. 1(e), i.e., the measurement just above the ionization region, i.e., $z = 3$ cm above the racetrack, as these values have been used for modeling the discharges.[4] The corresponding measured values are $F_{flux} = 5\%$ and 30%, respectively. Thus, the large variation in the ionized flux fraction ΔF_{flux} seen in Fig. 2 for different discharges operated in the fixed voltage mode can almost entirely be attributed to the change of α_t. The trends of β_t and ξ_{tn}/ξ_{ti} with increasing magnetic field strength appear to have a minor influence on F_{flux}.

In contrast, the fixed peak current discharges all have a close to constant value of α_t (see Fig. 5). The variations in F_{flux} shown in Fig. 1 can, therefore, be attributed to changes in β_t and ξ_{tn}/ξ_{ti}. For F_{flux} measured at $z = 3$ cm above the racetrack, we observe an almost constant value suggesting little or compensating variations of β_t and ξ_{tn}/ξ_{ti}. Contrary, F_{flux} evaluated at $z = 7$ cm above the center of the cathode target and the edge of the cathode target decreases with stronger magnetic field strength. From the slopes of the fits shown with a blue line in panels (a), (c), and (e) of Fig. 1, we observe that a weaker magnetic field correlates with a higher F_{flux}. This can be explained by a smaller target ion escape fraction $(1 - \beta_t)$ for stronger magnetic fields as suggested by Brenning *et al.*[10,35]. In addition, the value of the magnetic null point z_{null} that changes together with the magnetic field strength B_{rt} (see, e.g., Table I in Rudolph *et al.*[20]) could influence the axial spread of ions in a way that reduces the ion flux out of the ionization region at measurement positions. The reason why these parameters appear to have only a weak influence on fixed voltage discharges may be that they are shadowed by large variation in α_t for discharges operated in the fixed voltage mode.

The above analysis is similarly carried out in the following to understand changes in the deposition rate ΔR_{dep} with strengthening of the magnetic field from an eroding target. We note from Fig. 4 that the drop in R_{dep} when going from the weakest magnetic field to the strongest is much larger ($\Delta R_{dep} \approx -40\%$ to -50%) for the fixed voltage cases, compared to the change in the deposition rate for the fixed peak current cases ($\Delta R_{dep} \approx 10\%$) (Fig. 4). The drop in deposition rate for the fixed voltage cases can be attributed to the higher ionization probability α_t (Fig. 5). As the ionization probability grows due to higher peak discharge currents with target erosion, a considerable fraction of these ions is back-attracted. The fraction of ionized sputtered species that are back-attracted to the target (not to be confused with the probability of target ion back-attraction β_t) is

$$F_{back} = \alpha_t \beta_t. \tag{8}$$

For a quantitative estimate, we assume again an average back-attraction probability of $\beta_t = 0.85$ and a target species ionization probability of $\alpha_t = 0.45$ and 0.84 for weakest and strongest magnetic field configurations, respectively. This yields $F_{back} = 38\%$ and 71%, respectively. Thus, the fraction of sputtered species not back-attracted to the target, $1 - F_{back}$, decreases from 62% to 29%, a relative drop of 53%, very close to the measured drop in R_{dep} of $\Delta R_{dep} \approx -45\%$. The decrease in the deposition rate for the fixed voltage cases, can, thus, largely be explained by an increasing value for the probability of target atom ionization α_t with increasing target erosion (stronger magnetic field). Our conclusion here confirms the discussion by Greczynski and Hultman.[36] They demonstrate that the loss in the deposition rate for a HiPIMS discharge compared to a dcMS discharge with an equal average power scales with the peak discharge current density for a number of elemental target materials. Similar to our conclusion here, they attribute it to the increased ionization probability in combination with a high target ion back-attraction probability.

It should be noted that the internal discharge parameters α_t and β_t are normalized by the sputter rate.[4] Changes in the sputter rate, therefore, are not considered in Eq. (8) and in our discussion so far. However, a change in the composition of the ion current to the target changes the average sputter yield, even if the average power to the target is kept constant. As the peak discharge current increases with a strengthening of the magnetic field, the fraction of metal ions in the flux of metal and argon ions to the target increases.[19] Sputtering by metal ions, in general, has a different sputter yield compared to sputtering by Ar^+ ions; therefore, the average sputter rate may change. For the case of Ti, using the formulas given by Anders,[13] the sputter yield of an Ar^+ ion incident

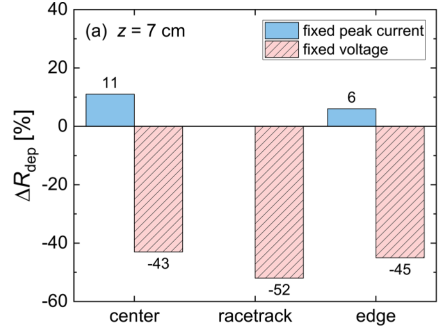

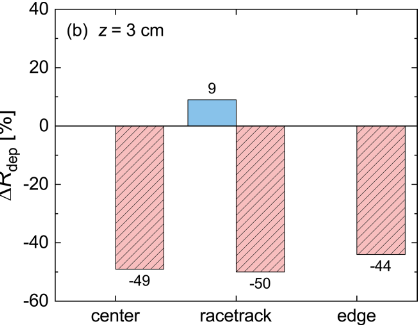

FIG. 4. Change in deposition rate ΔR_{dep} for the fixed peak current and fixed voltage mode operated discharges measured at height of (a) $z = 7$ cm and (b) $z = 3$ cm above the target surface. The change is measured from the fits in Fig. 1 between the weakest magnetic field configuration with $B_{rt} = 11.1$ mT and the strongest magnetic field configuration with $B_{rt} = 23.8$ mT.

© Author(s) 2022

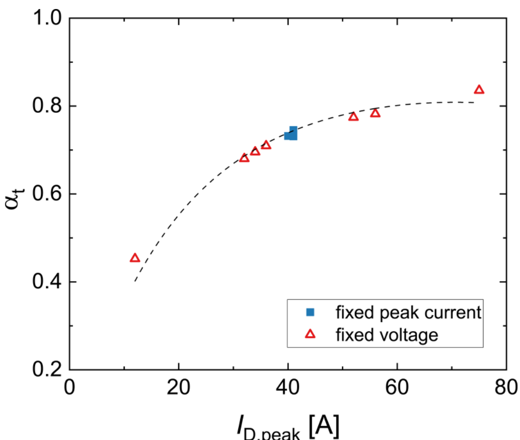

FIG. 5. Probability of sputtered target atom ionization α_t as a function of the peak discharge current. The data are obtained for discharges studied here by using the ionization region model (IRM). The black dashed curve is a fit through data points. The values indicate the measured magnetic field strength B_{rt} in the ionization region, 11 mm above the racetrack. Note that α_t according to this graph is a function of the peak discharge current alone, i.e., independent of magnetic field configuration. As a consequence, all the data points from discharges run in the fixed peak current mode are clustered in one point. Data reproduced from Rudolph *et al.* [20]

on a Ti target at 500 eV is $Y_{Ar^+\to Ti} = 0.67$, while that of a Ti^+ ion incident on a Ti target at 500 eV is $Y_{Ti^+\to Ti} = 0.58$. A higher fraction of metal ions in the ion current to the target with higher discharge currents is, therefore, expected to contribute to a reduced deposition rate when strengthening the magnetic field in the fixed voltage mode.

The change in the deposition rate ΔR_{dep} for the fixed peak current cases is much less dramatic with a change of only $\Delta R_{dep} \approx 10\%$ as shown in Fig. 4. For discharges operated in the fixed peak current mode, α_t remains constant because the peak discharge current remains constant.[20] However, the discharge voltage decreases with increasing magnetic field strength (Table I). For the following estimates, we assume that the deposition rate varies with the sputter yield Y or $R_{dep} \propto Y$. At the same time, Y is proportional to both the square root of the discharge voltage[13] and the pulse repetition frequency f; hence, $R_{dep}(t) \propto f(t)\sqrt{V_D(t)}$. Then, the relative change in deposition rate $\Delta R_{dep}(t)/R_{dep,0}$ can be expressed as

$$\frac{\Delta R_{dep}(t)}{R_{dep,0}} = \frac{f(t)\sqrt{V_D(t)} - f_0\sqrt{V_{D,0}}}{f_0\sqrt{V_{D,0}}} = \frac{f(t)}{f_0}\sqrt{\frac{V_D(t)}{V_{D,0}}} - 1, \qquad (9)$$

where $R_{dep,0}$ is the deposition rate and f_0 is the pulse repetition frequency at $t = 0$, i.e., the time at which the target is yet not eroded.

Inserting the discharge voltage and pulse repetition frequency of the discharge with the second-weakest magnetic field configuration ($V_{D,0} = 660$ V, $f_0 = 99$ Hz) and those of the discharge with the strongest magnetic field configuration ($V_D(t) = 510$ V, $f(t) = 143$ Hz, Table I), we obtain an expected relative change in the deposition rate of $\Delta R_{dep}(t)/R_{dep,0} = 27$ %. This is higher than the observed increase of about 10%. The difference could be explained by a changing discharge current waveform[9] that changes the average sputter rate from the target per pulse. In addition, changes in the transport parameters and the ion back-attraction probability β_t could introduce deviations from an assumed ideal proportionally between the sputter yield and the deposition rate.

From above discussion, we conclude that among the two modes of operating a HiPIMS discharge, the fixed voltage mode and the fixed peak current mode, the latter is the better choice. The reasons are that variations of the two flux parameters, ionized flux fraction and deposition rate, due to an eroding target and therefore a strengthening of the magnetic field, are limited when operating the discharge in fixed peak current mode.

Above, we mentioned a third mode of operating a HiPIMS discharge, namely, the fixed pulse power mode. We note that in this case, neither the peak discharge current nor the voltage during the pulse is controlled. If the control algorithm of the power supply is unknown, the influence of a changing magnetic field from an eroding target on the discharge voltage and the peak discharge current is uncertain and could lie anywhere between the trends for the two extreme cases, fixed peak current mode and fixed voltage mode. If the control algorithm is not known, this mode is not recommended.

As a perspective, we here point to the inverse trends in ionized flux fraction and deposition rate between the fixed peak current mode and the fixed voltage mode. These inverse trends suggest that there is an algorithm for which both the peak discharge current and voltage are adjusted in a way to maintain both the ionized flux fraction and deposition rate constant with target erosion.

V. CONCLUSION

To conclude, we discuss different modes of operating a HiPIMS discharge with the aim to keep the process reproducible in view of the unavoidable target erosion and the strengthening of the effective magnetic field at the target surface that goes along with erosion. The analysis shows that operating a discharge in the fixed peak current mode is superior to running a discharge in the fixed voltage mode. The reason is that a constant probability of target atom ionization can be maintained by keeping the peak discharge current constant. This limits the variations in the two flux parameters analyzed here, the ionized flux fraction and the deposition rate, under the influence of a strengthening magnetic field from an eroding target, which are of great importance for maintaining stable and reproducible deposition conditions.

ACKNOWLEDGMENTS

This work was partially supported by the Free State of Saxony and the European Regional Development Fund (Grant No. 100336119), the Icelandic Research Fund under Grant No. 196141, and the Swedish Government Strategic Research Area in Materials Science on Functional Materials at Linköping University (Faculty Grant SFO-Mat-LiU No. 2009-00971).

© Author(s) 2022

AUTHOR DECLARATIONS

Conflict of Interest

The authors have no conflicts to disclose.

DATA AVAILABILITY

The data that support the findings of this study are available from the corresponding author upon reasonable request.

REFERENCES

[1] J. T. Gudmundsson, Plasma Sources Sci. Technol. **29**, 113001 (2020).
[2] J. T. Gudmundsson, N. Brenning, D. Lundin, and U. Helmersson, J. Vacuum Sci. Technol. A **30**, 030801 (2012).
[3] *High Power Impulse Magnetron Sputtering: Fundamentals, Technologies, Challenges and Applications*, edited by D. Lundin, T. Minea, and J. T. Gudmundsson (Elsevier, Amsterdam, 2020).
[4] M. Rudolph, H. Hajihoseini, M. A. Raadu, J. T. Gudmundsson, N. Brenning, T. M. Minea, A. Anders, and D. Lundin, J. Appl. Phys. **129**, 033303 (2021).
[5] M. Lattemann, A. P. Ehiasarian, J. Bohlmark, P. Å. O. Persson, and U. Helmersson, Surf. Coat. Technol. **200**, 6495 (2006).
[6] M. Samuelsson, D. Lundin, J. Jensen, M. A. Raadu, J. T. Gudmundsson, and U. Helmersson, Surf. Coat. Technol. **202**, 591 (2010).
[7] M. Kateb, H. Hajihoseini, J. T. Gudmundsson, and S. Ingvarsson, J. Vac. Sci. Technol. A **37**, 031306 (2019).
[8] D. Lundin, M. Čada, and Z. Hubička, Plasma Sources Sci. Technol. **24**, 035018 (2015).
[9] H. Hajihoseini, M. Čada, Z. Hubička, S. Ünaldi, M. A. Raadu, N. Brenning, J. T. Gudmundsson, and D. Lundin, Plasma **2**, 201 (2019).
[10] N. Brenning, A. Butler, H. Hajihoseini, M. Rudolph, M. A. Raadu, J. T. Gudmundsson, T. Minea, and D. Lundin, J. Vac. Sci. Technol. A **38**, 033008 (2020).
[11] V. Kouznetsov, K. Macák, J. M. Schneider, U. Helmersson, and I. Petrov, Surf. Coat. Technol. **122**, 290 (1999).
[12] J. T. Gudmundsson, J. Fisher, B. P. Hinriksson, M. Rudolph, and D. Lundin, "Ionization region model of high power impulse magnetron sputtering of copper," Surf. Coat. Technol. 128189 (2022) (published online).
[13] A. Anders, J. Vac. Sci. Technol. A **28**, 783 (2010).
[14] A. Butler, N. Brenning, M. A. Raadu, J. T. Gudmundsson, T. Minea, and D. Lundin, Plasma Sources Sci. Technol. **27**, 105005 (2018).
[15] M. Rudolph, N. Brenning, M. A. Raadu, H. Hajihoseini, J. T. Gudmundsson, A. Anders, and D. Lundin, Plasma Sources Sci. Technol. **29**, 05LT01 (2020).
[16] T. Shimizu, M. Zanáška, R. P. Villoan, N. Brenning, U. Helmersson, and D. Lundin, Plasma Sources Sci. Technol. **30**, 045006 (2021).
[17] R. K. Waits, J. Vac. Sci. Technol. **15**, 179 (1978).
[18] C. Huo, D. Lundin, M. A. Raadu, A. Anders, J. T. Gudmundsson, and N. Brenning, Plasma Sources Sci. Technol. **22**, 045005 (2013).
[19] C. Huo, D. Lundin, J. T. Gudmundsson, M. A. Raadu, J. W. Bradley, and N. Brenning, J. Phys. D: Appl. Phys. **50**, 354003 (2017).
[20] M. Rudolph, N. Brenning, H. Hajihoseini, M. A. Raadu, T. M. Minea, A. Anders, D. Lundin, and J. T. Gudmundsson, J. Phys. D: Appl. Phys. **55**, 015202 (2022).
[21] J. Čapek, M. Hála, O. Zabeida, J. E. Klemberg-Sapieha, and L. Martinu, J. Appl. Phys. **111**, 023301 (2012).
[22] T. Kozák, Plasma Sources Sci. Technol. **21**, 025012 (2012).
[23] Z. Hubička, J. T. Gudmundsson, P. Larsson, and D. Lundin, in *High Power Impulse Magnetron Sputtering: Fundamentals, Technologies, Challenges and Applications*, edited by D. Lundin, T. Minea, and J. T. Gudmundsson (Elsevier, Amsterdam, 2020), pp. 49–80.
[24] D. V. Mozgrin, I. K. Fetisov, and G. V. Khodachenko, Plasma Phys. Rep. **21**, 400 (1995).
[25] J. T. Gudmundsson, J. Alami, and U. Helmersson, Surf. Coat. Technol. **161**, 249 (2002).
[26] P. M. Barker, E. Lewin, and J. Patscheider, J. Vac. Sci. Technol. A **31**, 060604 (2013).
[27] P. M. Barker, S. Konstantinidis, E. Lewin, N. Britun, and J. Patscheider, Surf. Coat. Technol. **258**, 631 (2014).
[28] O. Antonin, V. Tiron, C. Costin, G. Popa, and T. M. Minea, J. Phys. D: Appl. Phys. **48**, 015202 (2015).
[29] H. Hajihoseini, M. Čada, Z. Hubička, S. Ünaldi, M. A. Raadu, N. Brenning, J. T. Gudmundsson, and D. Lundin, J. Vac. Sci. Technol. A **38**, 033009 (2020).
[30] T. Kubart, M. Čada, D. Lundin, and Z. Hubička, Surf. Coat. Technol. **238**, 152 (2014).
[31] B. Window and N. Savvides, J. Vac. Sci. Technol. A **4**, 196 (1986).
[32] I. V. Svadkovski, D. A. Golosov, and S. M. Zavatskiy, Vacuum **68**, 283 (2003).
[33] D. J. Christie, J. Vac. Sci. Technol. A **23**, 330 (2005).
[34] J. Vlček and K. Burcalová, Plasma Sources Sci. Technol. **19**, 065010 (2010).
[35] N. Brenning, H. Hajihoseini, M. Rudolph, M. A. Raadu, J. T. Gudmundsson, T. M. Minea, and D. Lundin, Plasma Sources Sci. Technol. **30**, 015015 (2021).
[36] G. Greczynski and L. Hultman, Vacuum **124**, 1 (2016).

© Author(s) 2022